



Modification of graphene aerogel with titania nanotubes for efficient methylene blue adsorption kinetics

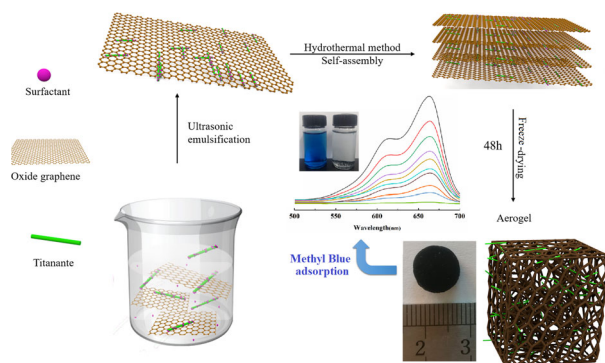
Hongli Liu^{1,2} · Bo Gao¹ · Wenjin Yuan¹ · Hongyan Li¹ · Jing Li¹ · Yajing Li¹ · Bo Zhang¹ · Zhong Chen^{1,3}

Received: 10 August 2020 / Accepted: 30 November 2020 / Published online: 16 January 2021
© The Author(s), under exclusive licence to Springer Science+Business Media, LLC part of Springer Nature 2021

Abstract

Titania nanotubes (TNTs) with high length–diameter ratio are incorporated into reduced graphene oxide (rGO) aerogel to modify the porous structure of the obtained rGO/TNTs aerogel for efficient methylene blue (MB) adsorption. A hydrothermal method along with freeze drying is applied for the preparation of the rGO/TNTs composite aerogel. The uniformly dispersed TNTs in rGO matrix can effectively support the network structure and hinder the π – π bonding interaction between graphene sheets, thus resulting in a three-dimensional mesoporous network with high specific surface area. The rGO/TNTs aerogel shows favorable adsorption property toward MB and the maximum adsorption capacity can be 380.7 mg g^{-1} with the adsorption efficiency of 92.2%. Besides, the adsorption kinetic analysis reveals that a dispersion process is found to be the rate-limiting step when the adsorbent dosage is low. With the increase of adsorbent content, chemical sorption such as the π – π interaction or the reaction of the polar functional groups between MB and rGO–TNTs-C aerogel becomes the rate-limiting step.

Graphical Abstract



Keywords Titania nanotubes · rGO aerogel · Methylene blue · Adsorption kinetics

Highlights

- TNTs are successfully employed for the pore structure regulation of rGO aerogel.
- The rGO/TNTs-C aerogel shows a maximum adsorption capacity of 380.7 mg g^{-1} towards MB.
- Diffusion of MB to the active sites of rGO aerogel is the rate-limiting step with low adsorbent dosage.
- Chemical sorption tends to be the rate-limiting step with the increase of adsorbent dosage.

✉ Wenjin Yuan
ywj407024846@126.com

¹ School of Materials Science and Engineering, Tianjin Chengjian University, Tianjin 300384, China

² Tianjin Key Laboratory of Building Green Functional Materials, Tianjin Chengjian University, Tianjin 300384, China

³ School of Materials Science and Engineering, Nanyang Technological University, 50 Nanyang Avenue, Singapore 639798, Singapore

1 Introduction

Dyes are widely used in pharmaceuticals, pesticides, textiles, and varnishes. However, the dyeing effluents discharge into water main cause many problems to the ecological environment and human health [1, 2]. Therefore, it is of great importance to remove these contaminants safely and effectively [3]. So far, a variety of technologies have been proposed to solve this problem, such as chemical precipitation [4], ultrafiltration [5], evaporation [6], ion exchange [7], solvent extraction [8], electrochemical treatment [9], photocatalysis [10], and adsorption [11–13]. Among these methods, adsorption has been considered as an efficient and economical process due to its low cost, simplicity, high efficiency, and wide-ranging availability [14, 15]. Thus, it is quite meaningful to design highly active adsorbents for effective dye adsorption. Recently, many studies have been reported for dye adsorption especially toward methylene blue (MB) [16–20].

Graphene, a honeycomb-arranged sp^2 carbon, displays high surface area, chemical stability, unique electronic and mechanical properties, and excellent adsorptivity [21–25], which is a promising adsorbent for water treatment. Compared with the powder graphene, graphene aerogel (GA) with well-defined interconnected porous networks in the form of block is more convenient for the adsorption of dyes in aqueous solution in consideration of the separation after adsorption, which can avoid the secondary pollution in water treatment. Wang et al. [26] fabricated a 3D reduced graphene oxide (rGO) aerogel and found that the adsorption capacity of GA varies from 115 to 1260 mg g^{-1} for different dyes. However, due to the uncontrollable agglomeration between the two-dimensional graphene sheets in the process of assembling into three-dimensional network, there is still a certain gap between the actual specific surface area and the theoretical value [27, 28]. Thus, appropriate modifications are urgently required to improve the comprehensive properties.

Titania nanotubes (TNTs) were first synthesized by Hoyer in 1996 via an electrochemical deposition in a porous aluminum oxide mold [29]. Then, it has been extensively studied due to the high specific surface area [30–35], good ion-exchangeable ability [36], and remarkable rapid and long-distance electron-transport capability [37]. Niu et al. found that TNTs show good adsorption property for the removal of organic molecules and radioactive toxic metal ions [38]. Taking these advantages into consideration, TNTs are expected to be a promising nanofiller for the modification of rGO aerogel and introducing more active sites toward dye adsorption.

In this paper, TNTs are employed to regulate the 3D network structure of the rGO aerogel through a simple hydrothermal self-assembly method. The incorporation of

TNTs can effectively hinder the strong hydrogen bonds and π - π interaction between the molecules and thus inhibit the uncontrollable agglomeration of graphene sheets, resulting in rGO/TNTs aerogel with high specific surface area and favorable MB adsorption property. The specific adsorption kinetics are also analyzed in detail, which can provide some ideas for other adsorption studies. Our results highlight the potential of TNTs to modify the structure of rGO aerogel and thus enhance the dye adsorption property, which provide new insight for the design of high-performance composites.

2 Experimental

2.1 Chemicals and materials

Graphite was purchased from Heilongjiang Aoyu Graphite Group Co., Ltd. Potassium permanganate (KMnO_4 , 99%) was purchased from Tianjin Chemical Plant. Concentrated H_2SO_4 , HCl , and cetyltrimethylammonium bromide (CTAB) were purchased from Sinopharm Group Chemical Reagent Co., Ltd. MB was purchased from Tianjin Fengchuan Chemical Reagent Science Co., Ltd. Hydrogen peroxide (H_2O_2), sodium nitrate (NaNO_3 , 99%), tertiary butyl alcohol ($\text{C}_4\text{H}_{10}\text{O}$), titanium dioxide (TiO_2), sodium hydroxide (NaOH), and distilled water were purchased from Tianjin Jiangtian Unified Technology Co., Ltd. The reagents used in this experiment do not need further purification.

2.2 Preparation of GO

GO was chemically synthesized following the modified Hummers method [39]. Overall, 10 g of natural graphite and 7.5 g of NaNO_3 were placed in a flask and 621 g of H_2SO_4 was added with stir in an ice water bath. 45 g of KMnO_4 was gradually added over about 1 h and the system was then reacted at 40 °C for 2 h. The obtained solution was diluted with 80 mL deionized water and kept at 90 °C for 1 h. After cooling down, 50 mL deionized water and a small amount of H_2O_2 solution were added and stood for 12 h. Then the suspension was washed with 5% HCl and deionized water to neutral, thus stable GO solution was obtained.

2.3 Preparation of TNTs

0.31 g of TiO_2 was added to 50 mL NaOH solution and reacted at a certain temperature with different stirring rate for 48 h in a Teflon-sealed autoclave. After cooling down, the sample was washed with deionized water and ethanol to remove impurities, and then dried at 72 °C for 6 h. The specific experimental parameters are shown in Table 1.

Table 1 Experimental parameters for the preparation of TNTs

Sample	Stirring rate (rpm)	Temperature (°C)	NaOH (M)
TNTs-1	650	150	5
TNTs-2	650	175	5
TNTs-3	650	150	10
TNTs-4	650	175	10
TNTs-5	780	150	10
TNTs-6	860	150	10

2.4 Preparation of rGO/TNTs aerogel

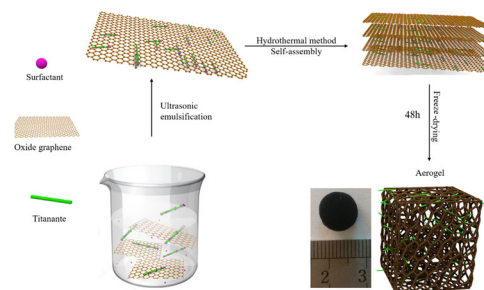
Overall, 2 mg of TNTs was added into 10 mL GO suspension (5 mg mL^{-1}) and ultrasonicated to form a uniform dispersion. In order to promote the dispersion process, surfactant CTAB was added. The mixture was then transformed into a Teflon-sealed autoclave and reacted at 180°C for 6 h. The obtained wet gel was then exchanged by tert-butanol during aging and followed by freeze drying. The rGO/TNTs aerogel was then obtained and denoted as rGO/TNTs-C. The sample without addition of CTAB was named rGO/TNTs. rGO aerogel was also prepared in the same condition without incorporation of TNTs. Fig. 1 schematically illustrates the preparation process.

2.5 Sample characterization

Fourier transform infrared (FT-IR) spectra of TNTs and rGO/TNTs aerogel were recorded by a FT-IR spectrometer (Nicolet 380) with KBr pellets in the wave number range of $4000\text{--}400 \text{ cm}^{-1}$. The phase compositions of the samples were analyzed by X-ray diffractometer (XRD, D8 Advance, Bruker AXS, Germany) with Cu $K\alpha$ radiation at a scan rate of $0.02^\circ \text{ s}^{-1}$. The morphologies of the samples were observed by field emission scanning electron microscope (SEM, JSM-7800F). Transmission electron microscope (TEM) was carried out on a JEOL JEM-2100F electron microscope at an acceleration voltage of 200 kV. The specific surface area and porosity of the aerogels were characterized by the pore structure analyzer (3H-2000PS1) and the samples were out-gassed at 180°C for 3 h before tests. Specific surface area and pore size distribution of the samples were calculated according to the Brunauer–Emmett–Teller (BET) method and Barrett–Joyner–Halenda method, respectively.

2.6 Adsorption experiments

The adsorption of MB from aqueous solution was conducted by batch adsorption experiments at 298 K. In order to avoid the interference caused by photocatalysis, the adsorption process was carried out in the darkness. The

**Fig. 1** Schematic illustration for the preparation process of rGO/TNTs aerogel

concentration of MB was detected by UV–vis spectrophotometer (TU-1900) at λ_{max} of 665 nm. The amount of MB adsorbed at time t ($q_t, \text{ mg g}^{-1}$) and at equilibrium ($q_e, \text{ mg g}^{-1}$) and the removal efficiency (%) were calculated by the following equations, respectively:

$$q_t = \frac{(C_0 - C_t)V}{m}, \quad (1)$$

$$q_e = \frac{(C_0 - C_e)V}{m}, \quad (2)$$

$$\text{Removal efficiency (\%)} = \frac{(C_0 - C_e)}{C_0} \times 100, \quad (3)$$

where C_0 , C_t , and C_e are initial, t time and equilibrium concentrations of MB (mg L^{-1}), respectively. m is the weight of the adsorbent (g) and V is the volume of MB solution (L).

3 Results and discussion

3.1 Composition and phase analysis

Figure 2a shows the FT-IR spectra of GO, TNTs, and rGO/TNTs aerogel. The absorption peaks at 3420 and 1080 cm^{-1} are assigned to the stretching vibration and bending vibration of --OH groups in GO and the absorption band at 1740 cm^{-1} is assigned to the stretching vibration of C=O groups, which indicate that there are numerous hydroxyl and carbonyl functional groups on the obtained GO. The formation of TNT is certified by the presence of the absorption peaks at 916 and 470 cm^{-1} , which are assigned to the Ti--O stretching vibration in OTi (OH)_2 molecule [40, 41] and the vibration of Ti--O in TiO_6 octahedrons [42, 43]. The absorption peak at 470 cm^{-1} can also be found in the rGO/TNTs aerogel, verifying the successful incorporation of TNTs. The decrease of the peak at 3400 cm^{-1} indicates that GO is reduced in the rGO/TNTs aerogel [26] during the hydrothermal process. The crystalline structures of GO, TNTs, and rGO/TNTs aerogels are studied by XRD. It can be seen from Fig. 2b that the diffraction peak at 12° is attributed to the $(0\ 0\ 2)$ plane of GO and the interlayer

Fig. 2 **a** FT-IR spectra and **b** XRD patterns of GO, TNTs, and rGO/TNTs aerogel

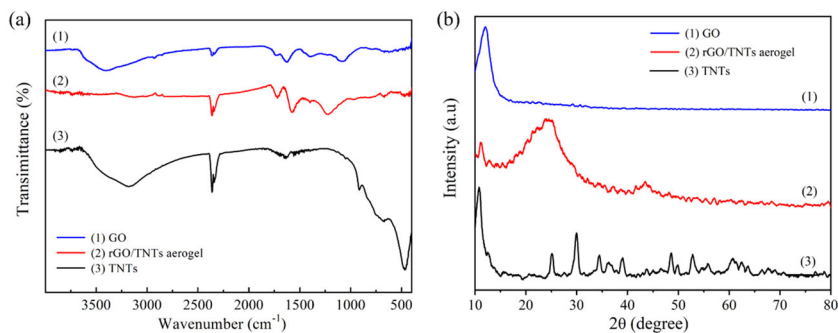
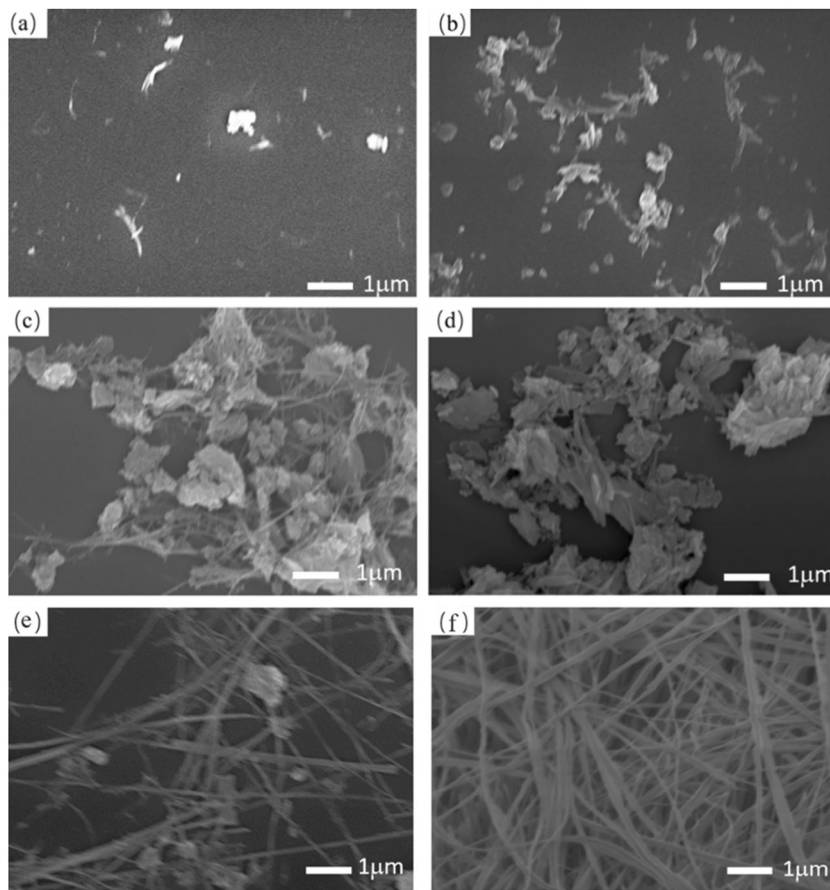


Fig. 3 SEM images of TNTs prepared under different conditions: **a** TNT-1, **b** TNTs-2, **c** TNTs-3, **d** TNTs-4, **e** TNTs-5, and **f** TNTs-6



spacing is calculated to be 0.73 nm by the Bragg equation [26]. The XRD spectrum of TNTs is consistent with the standard spectrum of monoclinic $\text{Na}_2\text{Ti}_3\text{O}_7$ (PDF 72–0148) and the peak at 10° is the typical diffraction peak of the layered titanate [44]. The peak at 25° in rGO/TNTs aerogel is assigned to carbon which further verifies the reduction of GO.

3.2 Morphology analysis

Figure 3 shows the morphology of TNTs obtained under different preparation conditions. It can be seen that at low NaOH concentration (Fig. 3a, b), the products show poor

morphology due to the incomplete reaction. With the increase of the NaOH concentration to 10 M, TNTs with a certain aspect ratio is initially formed, but there are still a lot of flakes. The reaction temperature shows no significant effect on the morphology of the product. It is worth noting that the obtained TNTs manifest a high aspect ratio with few impurities at faster stirring rate. This may be due to the fact that TiO_2 and NaOH solution can sufficiently contact with each other at high stirring speed, leading to a complete reaction. Meanwhile, the strong shear force under high stirring speed benefits for the formation of nanotubes. The optimal reaction conditions for the preparation of

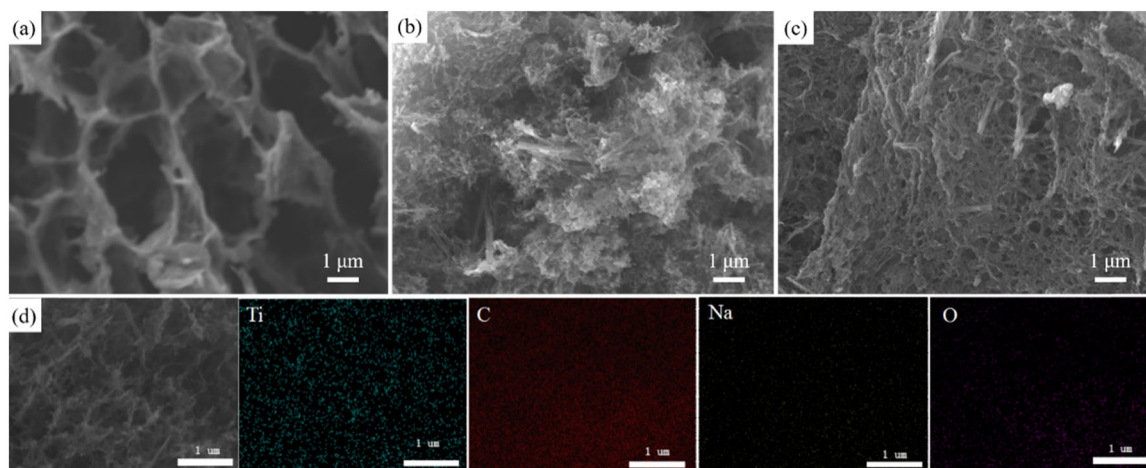
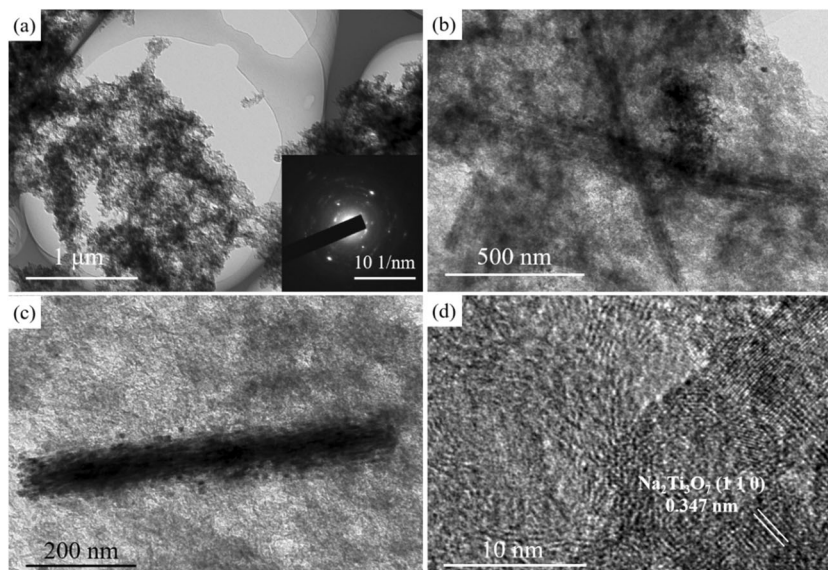


Fig. 4 SEM images of **a** rGO aerogel, **b** rGO/TNTs aerogel, **c** rGO/TNTs-C aerogel, and **d** the elemental mapping images of rGO/TNTs-C aerogel

Fig. 5 **a–c** Low-resolution and **d** high-resolution TEM images of rGO/TNTs-C aerogel (the inset in **a** shows the SAED pattern)



TNTs are 10 M NaOH at 150 °C with a stirring rate of 860 rpm.

In order to explore the influence of the addition of TNTs on the structure of the composite aerogel, the morphology of rGO, rGO/TNTs, and rGO/TNTs-C aerogels were investigated, respectively. As shown in Fig. 4, the original rGO aerogel has an irregular 3D porous structure with a large pore size. The addition of TNTs significantly reduces the pore size of the aerogel, which may result from the hydrogen bonding between TNTs and rGO aerogel. The obtained rGO/TNTs aerogel still shows an irregular 3D porous structure, but the TNTs in the aerogel are partially agglomerated. The rGO/TNTs-C aerogel obtained after CTAB modification manifests a more uniform pore structure, and TNTs are homogeneously distributed in the aerogel matrix with strong interfacial bonding (Fig. 4c). The coexistence and uniform distribution of Ti, C, Na, and O elements in rGO/TNTs-C aerogel are

validated by elemental mapping analysis, which further verifies the successful doping of TNTs. Thus, it can be safely concluded that the incorporation of TNTs shows obvious effect on the structure of rGO aerogel. The oxygenic groups, especially at the edges and wrinkles of the rGO aerogel can effectively interacted with the hydroxy groups in TNTs, thus leading to the regulation of the porous structure. Figure 5 shows the TEM images of the rGO/TNTs-C aerogel. It can be seen that the prepared TNTs are uniformly dispersed in the aerogel matrix. The lattice fringes observed with the interplanar spacing of 0.347 nm are assigned to the (1 1 0) plane of TNTs.

3.3 Pore structure analysis

Figure 6 shows the N₂ adsorption–desorption isotherms and the corresponding pore size distributions of rGO,

Fig. 6 **a** N_2 adsorption isotherms and **b** pore size distributions of the aerogels

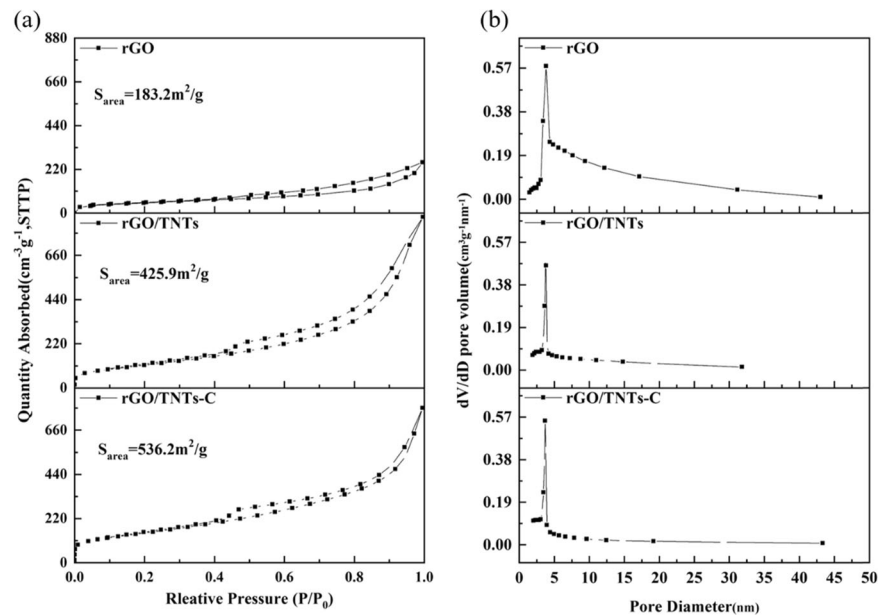


Table 2 Porous characteristics of the aerogels

Sample	S_{BET} ($m^2 g^{-1}$)	Average pore size (nm)	Pore volume ($cm^3 g^{-1}$)
RGO	183.2	6.95	0.36
RGO/TNTs	425.9	8.14	1.47
RGO/TNTs-C	536.2	7.14	1.29

rGO–TNTs, and rGO–TNTs-C aerogels. It can be seen that all the isotherms of the aerogels basically belong to type IV as defined by IUPAC, which is the characteristic of mesoporous materials [45]. Besides, they are in accordance with the type H3 hysteresis loops, indicating the slit-shaped pores in the composites [46], and their specific surface areas are 183.2, 425.9, and 536.2 $m^2 g^{-1}$, respectively. The specific porous characteristics of the aerogels are shown in Table 2. rGO aerogel shows the lowest specific surface area, which is caused by the uncontrollable agglomeration between the two-dimensional graphene sheets in the process of assembling into three-dimensional network. After the addition of TNTs, the specific surface area remarkably increases and shows further improvement with the modification of CTAB. This may be due to the fact that suitable incorporation of TNTs benefits for supporting of the network structure, and can effectively hinder the π – π bonding interaction between graphene sheets, thereby prohibiting their aggregation. The modification of CTAB ensures the uniform distribution of TNTs in the matrix and further optimizes the pore structure.

3.4 Adsorption property

The adsorption properties of TNTs, rGO, and rGO/TNTs-C aerogels toward MB are systematically studied. It can be seen from Fig. 7 that pure TNTs show poor adsorption property to MB. For rGO aerogel, although the adsorption rate is slow, the adsorption capacity at equilibrium is relatively high. The rGO/TNTs-C aerogel exhibits the best adsorption property with a faster adsorption rate. Their adsorption capacities are 198.6, 359.4, and 380.7 $mg g^{-1}$ with the removal efficiency of 49.7%, 89.8%, and 92.2%, respectively. The results indicate that the incorporation of TNTs can effectively improve the adsorption property of rGO aerogel through regulation of the porous structure. rGO/TNTs-C aerogel with high specific surface area can provide more active sites and increase the contact area between MB and the adsorbent, thereby promoting the adsorption process. Meanwhile, with the increase of adsorbent dosage, the adsorption rate of rGO/TNTs-C aerogel obviously increases and the removal efficiency also increases from 92.2 to 98.0%. This can be attributed to the increase of the adsorbent specific surface area and availability of more adsorption sites [47].

3.5 Adsorption kinetics

In order to identify the mechanism and the potential rate-controlling steps involved in the adsorption process, two kinetic models, pseudo first order and pseudo second order, are adopted to simulate and analyze the adsorption kinetics of the rGO/TNTs aerogels. The equation for pseudo first-order kinetics was introduced initially by Lagergren [48].

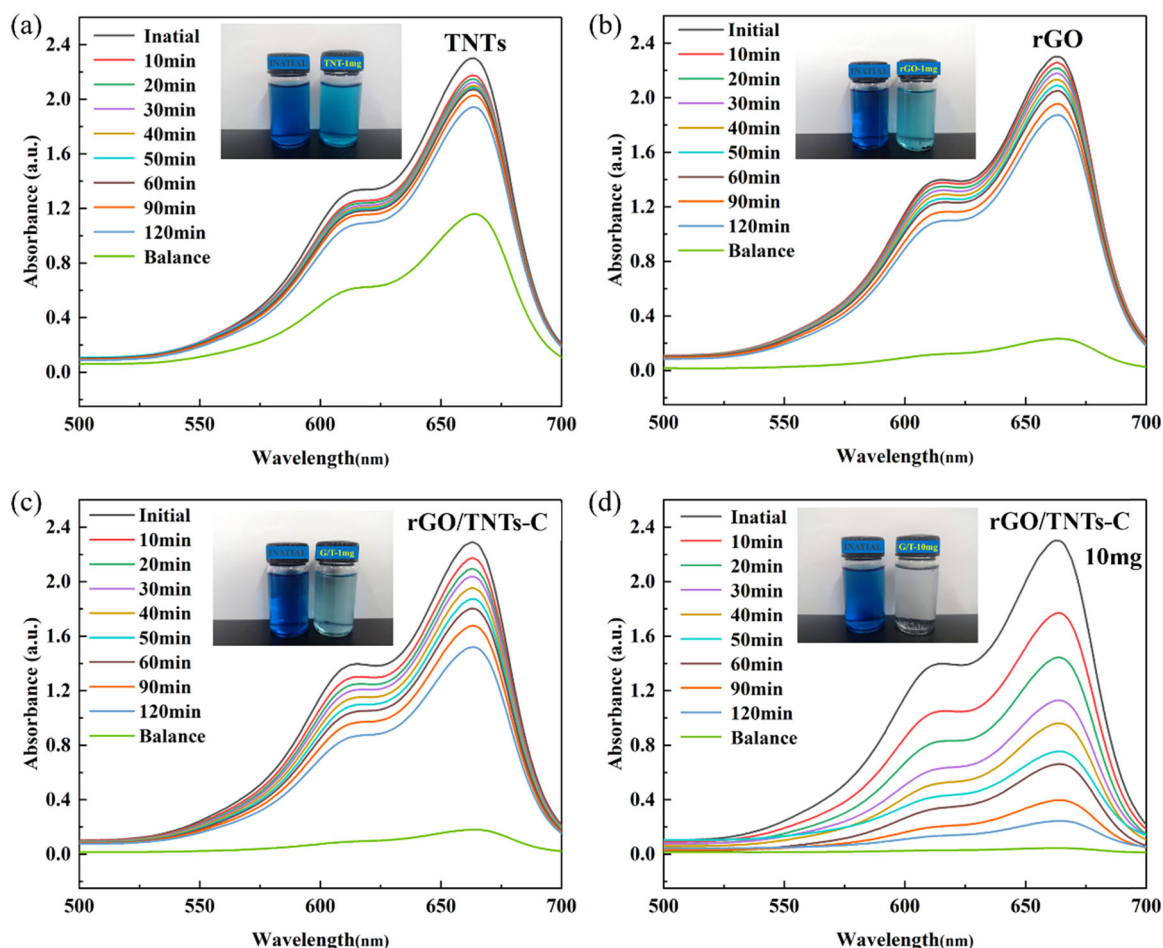


Fig. 7 UV-vis absorption spectra of MB solution by: **a** TNTs—1 mg, **b** rGO—1 mg, **c** rGO/TNTs-C—1 mg, and **d** rGO/TNTs-C—10 mg (inset shows the corresponding photographs of MB solutions before (left) and after (right) adsorption)

It is generally used in the form proposed by Ho and McKay [49]

$$\ln(q_e - q_t) = \ln q_e - k_1 t, \quad (4)$$

in which k_1 (min^{-1}) is the pseudo first-order rate constant and t (min) is the time.

The equation for pseudo second-order kinetics [50, 51] is generally employed in the form proposed by Ho and McKay [49]

$$\frac{t}{q_t} = \frac{t}{q_e} + \frac{1}{k_2 q_e^2}, \quad (5)$$

in which k_2 ($\text{g mg}^{-1} \text{min}^{-1}$) is the pseudo second-order rate constant.

Figure 8 shows the linear fitting plots of pseudo first-order and pseudo second-order kinetic models for adsorption of MB by TNTs, rGO, and rGO-TNTs-C aerogels with the adsorbent dosage of 1 mg and rGO-TNTs-C aerogel with dosage of 10 mg. The parameters q_e and k_1 for the pseudo first-order kinetic model (Eq. 4) could be obtained from the intercept and slope of the plots of $\ln(q_e - q_t)$ versus t . It can

be seen that the correlation coefficient of TNTs, rGO, and rGO-TNTs-C aerogels with 1 mg is 0.9785, 0.9947, and 0.9930, which suggests that the adsorption of MB fairly follows the pseudo first-order kinetic model. Besides, the calculated q_{e1} is also consistent with the experimental value q_{exp} , further verifies that it is suitable for rGO and rGO-TNTs-C aerogels. The results also manifest that the adsorption of MB is a dispersion controlled process in this system. For the pseudo second-order kinetic model (Eq. 5), the q_{e2} and k_2 can be obtained from the slope and intercept of the plots of t/q_t versus t . It can be seen that the correlation coefficient is relatively low and the calculated q_{e2} also shows a big variation from the experimental value q_{exp} , indicating that pseudo second-order kinetic model is not suitable for this system and chemisorption is not the rate-controlling step. So, when the adsorbent dosage is relatively low, a dispersion process is found to be the rate-limiting step [49]. With the increase of the rGO-TNTs-C aerogel content, the adsorption rate has been obviously improved and the adsorption kinetics have also changed. It can be seen that both of the kinetic models fit well and the pseudo second-

Fig. 8 Adsorption kinetics of MB adsorption: **a, c** pseudo first order and **b, d** pseudo second order

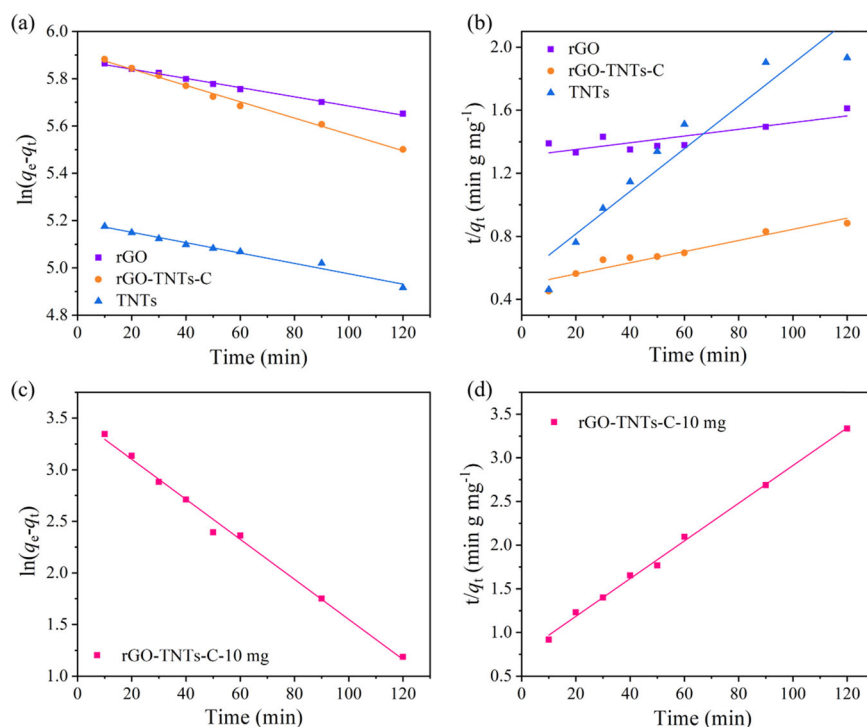


Table 3 Kinetic parameters of MB adsorption

Sample	q_{exp} (mg g^{-1})	Pseudo first order			Pseudo second order		
		q_{e1} (mg g^{-1})	k_1 (min^{-1})	r_1^2	q_{e2} (mg g^{-1})	k_2 ($\text{g mg}^{-1} \text{min}^{-1}$)	r_2^2
TNTs	198.6	180.3	0.0022	0.9785	73.9	3.3×10^{-4}	0.8977
rGO	359.4	357.4	0.0019	0.9947	469.5	3.5×10^{-6}	0.6765
rGO-TNTs-C	380.7	368.5	0.0035	0.9930	282.5	2.5×10^{-5}	0.9019
rGO-TNTs-C—10 mg	39.2	32.7	0.0194	0.9928	46.3	6×10^{-4}	0.9967

order kinetic model is better than the pseudo first-order kinetic model, which manifests that chemical sorption gradually becomes a rate-controlling step with the increase of adsorbent dosage. Thus, it can be safely concluded that when the adsorbent dosage is low, the adsorption process of MB is mainly controlled by the dispersion of MB molecules to the active sites of the aerogels. With the increase of the adsorbent content, chemical sorption or chemisorption involving valency forces through sharing or exchange of electrons such as the π - π chemical adsorption or the reaction of the polar functional groups between MB and rGO-TNTs-C aerogel becomes the rate-limiting step. The kinetic parameters obtained from these models are given in Table 3.

4 Conclusions

In summary, TNTs are successfully incorporated into rGO aerogel to regulate the pore structure of the aerogel, resulting in rGO/TNTs aerogel with high specific surface area and

favorable MB adsorption property. The effects of TNTs on the morphology, pore structure, and adsorption properties of rGO/TNTs aerogel are studied and the main conclusions are summarized as follows:

(1) The doping of TNTs can effectively prevent the agglomeration between graphene sheets in the process of assembling into three-dimensional network, thus resulting in a mesoporous rGO/TNTs aerogel with high specific surface area. The modification by CTAB ensures the uniform distribution of TNTs in the matrix and further optimizes the pore structure.

(2) rGO/TNTs-C aerogel shows the best adsorption property toward MB and the maximum adsorption capacity can be 380.7 mg g^{-1} with a quite high removal efficiency of 92.2%. Besides, the adsorption kinetic analysis indicates that the dispersion of MB molecules to the active sites of the aerogel is the rate-limiting step when the adsorbent dosage is low. With the increase of adsorbent content, chemical sorption or chemisorption involving valency forces through sharing or exchange of electrons such as the π - π chemical

adsorption or the reaction of the polar functional groups between MB and rGO–TNTs aerogel becomes the rate-limiting step. In brief, the rGO–TNTs aerogel with favorable adsorption property shows great potential in water treatment.

Acknowledgements This work was supported by the National Natural Science Foundation of China (No. 51772202).

Compliance with ethical standards

Conflict of interest The authors declare that they have no conflict of interest.

Publisher's note Springer Nature remains neutral with regard to jurisdictional claims in published maps and institutional affiliations.

References

- Acemioğlu B (2005) Batch kinetic study of sorption of methylene blue by perlite. *Chem Eng J* 106(1):73–81
- Al-Degs YS, Khraisheh MAM, Allen SJ, Ahmad MN (2009) Adsorption characteristics of reactive dyes in columns of activated carbon. *J Hazard Mater* 165(1–3):944–949
- Robinson T, McMullan G, Marchant R, Nigam P (2001) Remediation of dyes in textile effluent: a critical review on current treatment technologies with a proposed alternative. *Bioresour Technol* 77(3):247–255
- Sedighi F, Esmaili-Zare M, Sobhani-Nasab A, Behpour M (2018) Synthesis and characterization of CuWO₄ nanoparticle and CuWO₄/NiO nanocomposite using co-precipitation method; application in photodegradation of organic dye in water. *J Mater Sci Mater Electron* 29(16):13737–13745
- Vinodhini PA, Sudha PN (2016) Removal of heavy metal chromium from tannery effluent using ultrafiltration membrane. *Text Cloth Sustain* 2(1):5
- Lim SH, Rhee SW (2011) Drip and evaporation method for dye-TiO₂ nano junction formation in dye sensitized solar cells. *RSC Adv* 1(3):518–522
- Padmavathi R, Minnoli M, Sangeetha D (2014) Removal of heavy metal ions from waste water using anion exchange polymer membranes. *Int J Plast Technol* 18(1):88–99
- Pandit P, Basu S (2004) Dye and solvent recovery in solvent extraction using reverse micelles for the removal of ionic dyes. *Ind Eng Chem Res* 43(24):7861–7864
- Sala M, Lopez-Grimau V, Gutierrez-Bouzan C (2016) Photo-assisted electrochemical treatment of azo and phthalocyanine reactive dyes in the presence of surfactants. *Materials* 9(3):12
- Wang CC, Li J-R, Lv XL, Zhang YQ, Guo G (2014) Photocatalytic organic pollutants degradation in metal–organic frameworks. *Energy Environ Sci* 7(9):2831–2867
- Lee JY, Chen CH, Cheng S, Li HY (2016) Adsorption of Pb(II) and Cu(II) metal ions on functionalized large-pore mesoporous silica. *Int J Environ Sci Technol* 13(1):65–76
- Li J, Gong JL, Zeng GM, Zhang P, Song BA, Cao WC et al. (2018) Zirconium-based metal organic frameworks loaded on polyurethane foam membrane for simultaneous removal of dyes with different charges. *J Colloid Interf Sci* 527:267–279
- Ghaffar A, Zhang L, Zhu X, Chen B (2018) Porous PVDF/GO nanofibrous membranes for selective separation and recycling of charged organic dyes from water. *Environ Sci Technol* 52(7):4265–4274
- Rafatullah M, Sulaiman O, Hashim R, Ahmad A (2010) Adsorption of methylene blue on low-cost adsorbents: a review. *J Hazard Mater* 177(1–3):70–80
- Sharma YC, Uma, Sinha ASK, Upadhyay SN (2010) Characterization and adsorption studies of *Cocos nucifera* L. activated carbon for the removal of methylene blue from aqueous solutions. *J Chem Eng Data* 55(8):2662–2667
- Hu N, Chen C, Tan J, Wang W, Wang C, Fan H et al. (2020) Enhanced adsorption of methylene blue triggered by the phase transition of thermoresponsive polymers in hybrid interpenetrating polymer network hydrogels. *ACS Appl Polym Mater* 2(8):3674–3684
- Wahlstrom N, Steinhagen S, Toth G, Pavia H, Edlund U (2020) Ulvan dialdehyde-gelatin hydrogels for removal of heavy metals and methylene blue from aqueous solution. *Carbohydr Polym* 249:116841
- Mishra SP, Patra AR, Das S (2020) Methylene blue and malachite green removal from aqueous solution using waste activated carbon. *Biointerface Res Appl Chem* 11(1):7410–7421
- Deng W, Tang S, Zhou X, Liu Y, Liu S, Luo J (2020) Honeycomb-like structure-tunable chitosan-based porous carbon microspheres for methylene blue efficient removal. *Carbohydr Polym* 247:116736
- Feng M, You W, Wu Z, Chen Q, Zhan H (2013) Mildly alkaline preparation and methylene blue adsorption capacity of hierarchical flower-like sodium titanate. *ACS Appl Mater Interfaces* 5(23):12654–12662
- Geim AK, Novoselov KS (2007) The rise of graphene. *Nat Mater* 6(3):183–191
- Zhang YB, Tan YW, Stormer HL, Kim P (2005) Experimental observation of the quantum Hall effect and Berry's phase in graphene. *Nature* 438(7065):201–204
- Fal'ko VI, Geim AK (2007) Graphene: emerging matter in two dimensions. *Eur Phys J Spec Top* 148:1–3
- Kopelevich Y, Esquinazi P (2007) Graphene physics in graphite. *Adv Mater* 19(24):4559–4563
- Nair RR, Blake P, Grigorenko AN, Novoselov KS, Booth TJ, Stauber T et al (2008) Fine structure constant defines visual transparency of graphene. *Science* 320(5881):1308
- Wang JL, Shi ZX, Fan JC, Ge Y, Yin J, Hu GX (2012) Self-assembly of graphene into three-dimensional structures promoted by natural phenolic acids. *J Mater Chem* 22(42):22459–22466
- Wang RH, Xu CH, Sun J, Gao L (2014) Three-dimensional Fe₂O₃ nanocubes/nitrogen-doped graphene aerogels: nucleation mechanism and lithium storage properties. *Sci Rep* 4:7
- Qian YQ, Ismail IM, Stein A (2014) Ultralight, high-surface-area, multifunctional graphene-based aerogels from self-assembly of graphene oxide and resol. *Carbon* 68:221–231
- Hoyer P (1996) Formation of a titanium dioxide nanotube array. *Langmuir* 12(6):1411–1413
- Bavykin DV, Parmon VN, Lapkin AA, Walsh FC (2004) The effect of hydrothermal conditions on the mesoporous structure of TiO₂ nanotubes. *J Mater Chem* 14(22):3370–3377
- Yu JG, Yu HG (2006) Facile synthesis and characterization of novel nanocomposites of titanate nanotubes and rutile nanocrystals. *Mater Chem Phys* 100(2–3):507–512
- Yu JG, Yu HG, Cheng B, Trapalis C (2006) Effects of calcination temperature on the microstructures and photocatalytic activity of titanate nanotubes. *J Mol Catal A-Chem* 249(1–2):135–142
- Chen XB, Cao S, Weng XL, Wang HQ, Wu ZB (2012) Effects of morphology and structure of titanate supports on the performance of ceria in selective catalytic reduction of NO. *Catal Commun* 26:178–182

34. Mozia S, Borowiak-Palen E, Przepiorski J, Grzmil B, Tsumura T, Toyoda M et al. (2010) Physico-chemical properties and possible photocatalytic applications of titanate nanotubes synthesized via hydrothermal method. *J Phys Chem Solids* 71(3):263–272
35. Song FJ, Zhao YX, Zhong Q (2013) Adsorption of carbon dioxide on amine-modified TiO₂ nanotubes. *J Environ Sci* 25(3):554–560
36. Kim M, Hwang SH, Lim SK, Kim S (2012) Effects of ion exchange and calcinations on the structure and photocatalytic activity of hydrothermally prepared titanate nanotubes. *Cryst Res Technol* 47(11):1190–1194
37. Rajeshwar K, Osugi ME, Chanmanee W, Chenthamarakshan CR, Zaroni MVB, Kajitvichyanukul P et al. (2008) Heterogeneous photocatalytic treatment of organic dyes in air and aqueous media. *J Photochem Photobiol C-Photochem Rev* 9(4):171–192
38. Niu HY, Wang JM, Shi YL, Cai YQ, Wei FS (2009) Adsorption behavior of arsenic onto protonated titanate nanotubes prepared via hydrothermal method. *Microporous Mesoporous Mater* 122(1–3):28–35
39. Hirata M, Gotou T, Horiuchi S, Fujiwara M, Ohba M (2004) Thin-film particles of graphite oxide 1: high-yield synthesis and flexibility of the particles. *Carbon* 42(14):2929–2937
40. Shao LM, Zhang LN, Chen MH, Lu H, Zhou MF (2001) Reactions of titanium oxides with water molecules. a matrix isolation FTIR and density functional study. *Chem Phys Lett* 343(1–2):178–184
41. Chen YC, Lo SL, Kuo J (2010) Pb(II) adsorption capacity and behavior of titanate nanotubes made by microwave hydrothermal method. *Colloids Surf A* 361(1–3):126–131
42. Wang W, Zhang JW, Huang HZ, Wu ZS, Zhang ZJ (2008) Surface-modification and characterization of H-titanate nanotube. *Colloids Surf A* 317(1–3):270–276
43. Wang H, Wang HL, Jiang WF, Li ZQ (2009) Photocatalytic degradation of 2,4-dinitrophenol (DNP) by multi-walled carbon nanotubes (MWCNTs)/TiO₂ composite in aqueous solution under solar irradiation. *Water Res* 43(1):204–210
44. Liu F, Jin YJ, Liao HB, Cai L, Tong MP, Hou YL (2013) Facile self-assembly synthesis of titanate/Fe₃O₄ nanocomposites for the efficient removal of Pb²⁺ from aqueous systems. *J Mater Chem A* 1(3):805–813
45. Tu TH, Cam PTN, Huy LVT, Phong MT, Nam HM, Hieu NH (2019) Synthesis and application of graphene oxide aerogel as an adsorbent for removal of dyes from water. *Mater Lett* 238:134–137
46. Sing KSW, Everett DH, Haul RAW, Moscou L, Pierotti RA, Rouquerol J et al. (1985) Reporting physisorption data for gas-solid systems with special reference to the determination of surface area and porosity (Recommendations 1984). *Pure Appl Chem* 57:603–619
47. Royer B, Cardoso NF, Lima EC, Vaghetti JCP, Simon NM, Calvete T et al. (2009) Applications of Brazilian pine-fruit shell in natural and carbonized forms as adsorbents to removal of methylene blue from aqueous solutions—kinetic and equilibrium study. *J Hazard Mater* 164(2–3):1213–1222
48. Lagergren SY (1898) Zur Theorie der sogenannten Adsorption gelöster Stoffe. *K sven vetenskapskad handl* 24:1–39
49. Ho YS, McKay G (1999) Pseudo-second order model for sorption processes. *Process Biochem* 34(5):451–465
50. Blanchard G, Maunaye M, Martin G (1984) Removal of heavy metals from waters by means of natural zeolites. *Water Res* 18(12):1501–1507
51. Gosset T, Trancart JL, Thévenot DR (1986) Batch metal removal by peat. *Kinet Thermodyn Water Res* 20(1):21–26